Optical Engineering

SPIEDigitalLibrary.org/oe

Thermally induced damage studies with shaped light

Bathusile N. Masina
Bonex Mwakikunga
Andrew Forbes

Downloaded From: http://spiedigitallibrary.org/ on 08/21/2013 Terms of Use: http://spiedl.org/terms

Thermally induced damage studies with shaped light

Bathusile N. Masina
CSIR National Laser Centre
P. O. Box 395, Pretoria 0001, South Africa
and
University of KwaZulu-Natal
School of Physics, Private Bag X54001
Durban 4000, South Africa

Bonex Mwakikunga
CSIR National Centre for Nano-Structured Materials
P. O. Box 395, Pretoria 0001, South Africa

Andrew Forbes
CSIR National Laser Centre
P. O. Box 395, Pretoria 0001, South Africa
and
University of KwaZulu-Natal
School of Physics, Private Bag X54001
Durban 4000, South Africa
E-mail: aforbes1@csir.co.za

Abstract. We outline an all-optical and noncontact approach for controlled laser heating and measurement of the resultant temperature distribution at the surface of a material, respectively. We show how the boundary conditions of the heating problem may be controlled optically through shaping of the pump light and use the examples of both Gaussian and flat-top beams. These two beams, together with appropriate nonoptical boundary control, allow for the laser-induced thermal study of materials with and without thermal stress. We illustrate the technique on an industrial diamond sample where a gradient and uniform temperature profile on the surface of the diamond was successfully created and measured. We use the technique to study the thermally induced degradation of industrial diamond in a controlled manner. © *2013 Society of Photo-Optical Instrumentation Engineers (SPIE)* [DOI: 10.1117/1.OE.52.4.044301]

Subject terms: laser heating; thermal stress; polycrystalline diamond tools.

Paper 130067 received Jan. 15, 2013; revised manuscript received Mar. 12, 2013; accepted for publication Mar. 18, 2013; published online Apr. 8, 2013.

1 Introduction

Laser heating of material surfaces has emerged as a powerful tool for studies of material residual stresses, tool wear, and surface dynamics, as well as in surfaces processing and chemical analysis.[1–3] Measuring surface temperatures during laser heating is important for correctly interpreting the observed phenomena and describing forces behind material-property changes of heated materials. As scientists try to achieve a better understanding of the phenomena and try to better control and predict them, accurate measurement of temperature becomes more critical. Scientists have attempted to measure temperature with various techniques[4–6] that can be classified into three categories[7,8] depending on the nature of contact between the measuring device and the solid, liquid, or gaseous medium of interest: (1) contact, (2) semicontact, and (3) noncontact.

A contact technique is when the measuring device is in direct contact with the medium of interest, such as with thermocouples.[8,9] Thermocouples are commonly used owing to their low cost, simplicity, robustness, size, and temperature range. Their problem is the intimate contact with the surface, which affects the local surface energy balance and thus the very temperature one wishes to measure.[10] The small sampling area of such sensors is also an issue and is affected by radiant energy exchange that can cause the measured temperature to differ from the surrounding surface.[11] These sensors measure only the mean temperature over the entire contact area, whereas high local or flash temperatures, which can may occur for a short period of time, cannot be observed.[12,13] The sensors require periodic recalibration due to electromagnetic interference and environmental degradation.[8]

A semicontact technique is when the medium of interest is treated in some manner to enable remote observation, for example, surface coatings whose color changes with temperature. Semicontact techniques such as temperature-sensitive paints are generally limited to temperatures <380 K. Additionally, thermal paints are inappropriate for time-resolved measurements, and they allow an estimation of the peak temperature only, which is indicated by an irreversible color change of the paint.[14] However, thermographic phosphors offer a semicontact technique with spatial and temporal resolution over a broad temperature range, provided they are carefully handled.[15,16]

An alternative is a noncontact technique which avoids the aforementioned problems because the medium of interest is observed remotely. For example a noncontact infrared (IR) thermographic system can provide spatial and temporal measurements with good resolution and without interfering with the heating process.[17–19] This system measures temperature based on thermal radiation in the IR spectrum. Generally, it may include an optical system, a detector, and a control and analysis system. An excellent review of the technique can be found in Ref. 20.

Laser-based systems are ideal for creating the intensities required to raise the temperature of an object under study. In a typical setup, a laser beam is focused onto the absorbing object, causing the object's temperature to increase. The advantage of using the laser to raise the temperature of the object is that the laser beam can easily be adjusted and controlled to deliver intense heat over a small or a large area of the object, for desired periods of time, by varying the laser beam parameters such as spot size and laser power. The laser beam intensity profiles can also be shaped to allow for control of the heat source at the sample.

Laser beam shaping is the process of redistributing the irradiance and phase of a beam of optical radiation and

0091-3286/2013/$25.00 © 2013 SPIE

Downloaded From: http://spiedigitallibrary.org/ on 08/21/2013 Terms of Use: http://spiedl.org/terms

has been reviewed extensively to date.[21,22] The laser beam intensity profile can be shaped with either amplitude or phase modulation of the beam by using diffractive optical elements (DOEs),[23] aperturing of the input laser beam,[24] and so on. Amplitude modulation is effective in beam shaping but has the drawback of wasting significant amounts of the laser energy; phase modulation is much more efficient for commercial uses and is virtually lossless. The shaped laser beam profile may be arbitrary, including rectangular, circular, triangular, ring-shaped, and flat-top, to name but a few.

In this work, we make use of laser beam shaping to control the heat source term in thermal studies and use a noncontact measurement technique to monitor the impact of the source term in real time. To date, there have been no thermal studies that exploit laser beam shaping to control the heat source term. In this study, we implement an all-optical system for both laser heating and measuring of the resulting temperature distribution of a body. We make use of a DOE in conjunction with a Fourier-transforming lens to transform a Gaussian beam profile into a flat-top beam profile. The laser beam can therefore be customized in intensity profile at the plane of the sample to be heated. The ability to heat the diamond tool with two laser beam profiles and two optical setups will be demonstrated. A model for the temperature on the surface of the diamond tool was developed and shows qualitative agreement with experimental data. It will be shown that it is possible to engineer the boundary conditions and initial beam such that a uniform or gradient in temperature can be created, allowing the study of thermal effects with or without thermal stresses. We demonstrate the usefulness of such a technique with the example of thermally induced damage in an industrial diamond sample.

2 Temperature Distribution Model

In this study, an analytical model based on the heat diffusion equation is developed to analyze temperature distribution in a material irradiated by a laser. For the moment, we restrict ourselves to cylindrical symmetry, although conversion to other geometries is well known,[25] and we assume that most of the heating occurs near the surface of the material (since the absorption of nontransparent objects is usually very high). Further, to aid simplification, we assume that thermal parameters of the material of interest in the considered temperature range are constant and temperature independent.[26]

To find the dynamic temperature distribution on the surface of the sample, we solve the heat diffusion equation with a nonzero source term:[27]

$$\frac{\partial U(r,t)}{\partial t} - D\nabla^2 U(r,t) = Q(r), \tag{1}$$

with diffusivity $D = k/\rho C_p$ and where $U(r,t)$ is the temperature on the surface of the sample. Here ρ is the density, k is the conductivity, C_p is the heat capacity, and $Q(r)$ is the source term for a nonzero absorption of the laser light, α. If the source term is a laser beam with an intensity distribution $I(r)$, then[25,28]

$$Q(r) = \frac{I(r)\alpha}{\rho l C_p}. \tag{2}$$

For a Gaussian laser beam of radius w and power P_0, this becomes

$$Q(r) = \frac{2P_0\alpha \exp\left(\frac{-2r^2}{w^2}\right)}{\rho l C_P \pi w^2}. \tag{3}$$

In the case when a flat-top beam is used, the source term is given by[29]

$$Q(r) = \frac{P_0\alpha}{\rho l C_P \pi w^2}. \tag{4}$$

Clearly, varying the total power of the laser or the beam size or the distribution of power in the beam (intensity profile) will vary the source term. The nonhomogenous Eq. (1) can be solved using Green's functions, which leads to an integral solution given by[30]

$$U(r,t) = \int_0^t \int_0^a Q(\xi,\tau) G(r,\xi,t-\tau)\mathrm{d}\xi\mathrm{d}\tau, \tag{5}$$

with

$$G(r,\xi,t) = \sum_{m=1}^{\infty} \frac{2\xi}{a^2 J_1^2(\alpha_m)} J_0\left(\alpha_m \frac{r}{a}\right) J_0\left(\alpha_m \frac{\xi}{a}\right) \times \exp\left(-\frac{D\alpha_m^2 t}{a^2}\right) \tag{6}$$

in the case of a constant temperature boundary condition $[U(a,t) = 0]$ and

$$G(r,\xi,t) = \frac{2}{a^2}\xi + \frac{2}{a^2}\sum_{m=1}^{\infty} \frac{\xi}{J_0^2(\alpha_m)} J_0\left(\alpha_m \frac{r}{a}\right) J_0\left(\alpha_m \frac{\xi}{a}\right) \times \exp\left(-\frac{D\alpha_m^2 t}{a^2}\right) \tag{7}$$

when the temperature of the boundary may vary but the heat flow across the surface is zero $[\partial U/\partial r = 0$ at $r = a]$. The α_m terms are positive zeros of the first order of the Bessel function, $J_1(\alpha_m) = 0$. Here a is the sample radius, J_x refers to a Bessel function of order x, and r is the radial coordinate. From Eq. (5), the temperature profile as function of time on the surface of the sample can be determine by substituting the source term given in Eq. (3) and the Green's function given in Eqs. (6) and (7), respectively. The temperature profile as a function of time on the surface of the sample may be found to be

$$U(r,t) = U_0 + \frac{4P_o\alpha}{kl\pi w^2} \sum_{m=1}^{\infty} \frac{J_o\left(\alpha_m \frac{r}{a}\right)\left[1 - \exp\left(-\frac{D\alpha_m^2 t}{a^2}\right)\right]}{\alpha_m^2 J_1^2(\alpha_m)} \times \int_0^a \exp\left(-\frac{2\xi^2}{w^2}\right) \xi J_o\left(\alpha_m \frac{\xi}{a}\right)\mathrm{d}\xi, \tag{8}$$

Downloaded From: http://spiedigitallibrary.org/ on 08/21/2013 Terms of Use: http://spiedl.org/terms

$$U(r,t) = U_0 + \frac{tP_0\alpha}{l\rho\pi a^2 C_P}\left[1 - \exp\left(\frac{-2a^2}{\omega^2}\right)\right] + \frac{4P_0\alpha}{l\pi\omega^2 k}\sum_{m=1}^{\infty}\frac{J_0\left(\frac{\alpha_m r}{a}\right)\left[1 - \exp\left(\frac{-D\alpha_m^2 t}{a^2}\right)\right]}{\alpha_m^2 J_o^2(\alpha_m)} \times \int_0^a \exp\left(\frac{-2\xi^2}{w^2}\right)\xi J_o\left(\alpha_m\frac{\xi}{a}\right)\mathrm{d}\xi. \quad (9)$$

Here Eq. (8) refers to the constant-boundary-temperature case, and Eq. (9), to the zero-heat-flow case. The beam size along with beam power determines the power intensity distribution, and in this study various beam sizes, irradiating durations, and beam profiles were used to alter the heating characteristics. Some typical results of the calculated surface temperature under these conditions are shown in Fig. 1. Results show that the surface temperature distributions are uniform due to the zero-heat-flow assumption but show a strong gradient due to the constant-boundary-temperature assumption. As expected, the peak surface temperature increases as the laser beam power increases and is higher for smaller focused spots of intense light. A smaller laser beam size results in a high surface temperature.

2.1 *Diamond Tool*

One of the questions that we address here is whether thermally induced problems in some materials arise as a result of how hot the object is rather than the gradient of temperature across the material. One might anticipate that the former is due to uniform temperature profile, whereas the latter is due to gradient temperature profile. In this work, a synthetic diamond tool was chosen, a material that has found widespread use for drill bits in the mining industry. The drill bits are fitted with the diamond tool for a significant portion of the total footage drilled and are popularity for their effectiveness in drilling soft to medium formations at relativity high penetration rates.[31] However, the drill bits reach very high temperatures during a typical drilling process due to friction, with the efficiency of the material decreasing rapidly at temperatures exceeding 700°C to 750°C, and it is thought that the damage is induced by thermal stress.[32] The diamond tool comprises a polycrystalline diamond (PCD) layer on a supporting tungsten carbide (WC) substrate that is sintered at high temperature and high pressure (HTHP); the origin of this diamond has been discussed previously.[33] The HTHP diamond tool used in this study was deposited on a 15-mm-diameter cylindrical alloy substrate containing WC with trace elements of iron (Fe) and cobalt (Co). The total thickness of the sample was 15 mm, where WC is 12 mm thick and PCD is 3 mm thick, as shown in the inset of Fig. 2.

2.2 *Laser Heating and Temperature Measurement of the Diamond Tool*

Here we demonstrate how to raise the temperature of the diamond tool and measure it. Figure 3 shows the schematic optical system layout of this study. A continuous wave CO_2 laser (Synrad D48-2-115) was used as the laser heating source in the experiment. A helium-neon laser was aligned to be colinear with the CO_2 beam to facilitate alignment of

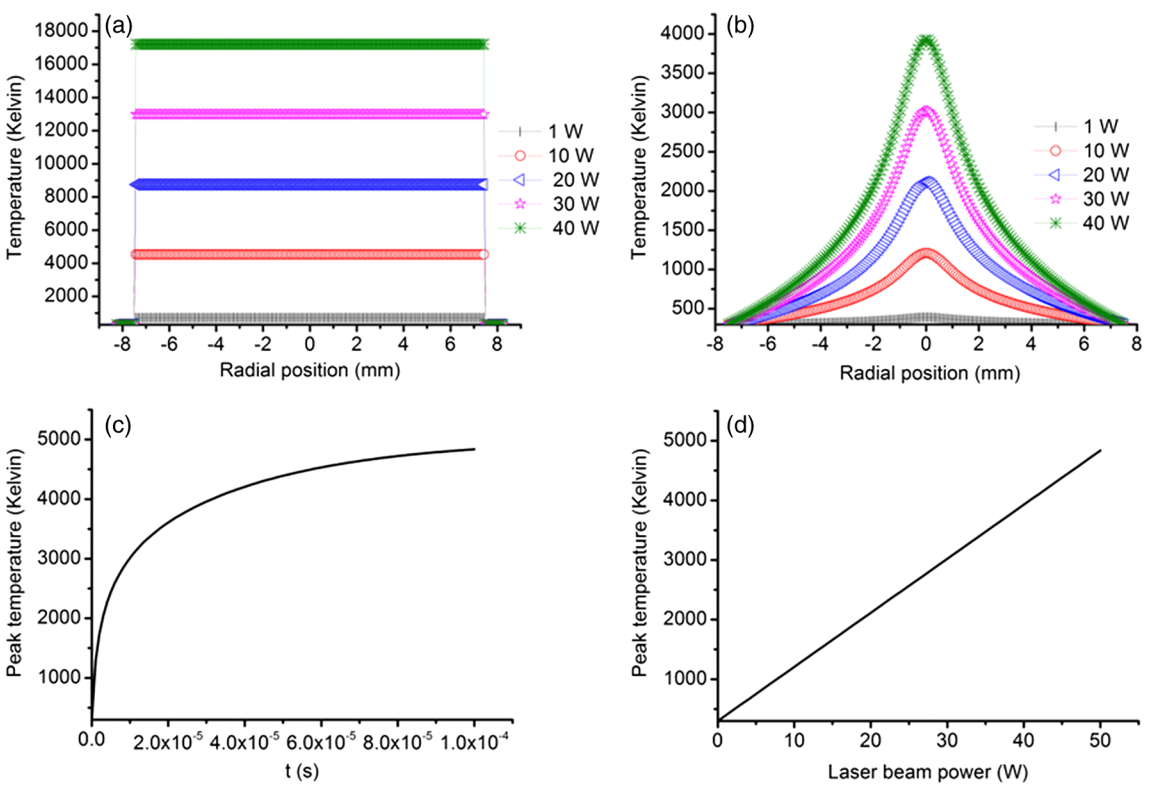

Fig. 1 Temperature profile across the surface sample. (a) Insulator holder results. (b) Copper-cooled holder results. (c) For both cases, temperature rises as time increases and stabilizes after a few minutes. (d) For both cases, temperature rises as laser beam power increases. Laser beam parameters and material properties used for these simulations: $t = 0.0001$ s, $w = 1$ mm, $k = 530$ W/mK^{-1}, $\rho = 4000$ kg/m^3, and $C_p = 0.521$ J/kg K^{-1}.

Downloaded From: http://spiedigitallibrary.org/ on 08/21/2013 Terms of Use: http://spiedl.org/terms

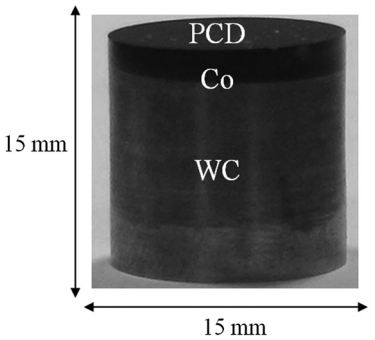

Fig. 2 The diamond sample.

the invisible IR CO_2 beam throughout the optical system. The DOE element was designed to work at a specific wavelength of 10.6 μm and a beam radius of 7 mm. The laser beam was delivered through suitable optical elements to produce a beam radius of 7 mm, with a near-flat wavefront at a focusing lens (ZnSe) with focal length 250 mm. The DOE beam shaping element and a Fourier transforming lens were placed at the position where the 7-mm beam radius was located, and the Gaussian beam could be reshaped to a flat-top beam at the same plane after the lens, as shown in Fig. 4(a) and 4(b), respectively. The power delivered to the sample could be varied between 1 and 40 W with the polarization-based attenuator, and the size of the beam at the sample could be chosen depending on the distance after the lens. An 88% reflecting beam splitter allowed continuous monitoring of the laser power over the duration of the experiment, and the laser beam profiles at the sample were measured with a pyro-electric camera (Spiricon Pyrocam III).

We carried out two sets of experiments: (1) In the first experiment, the temperature across the object was kept constant, with no gradient and therefore no stresses, and (2) In the second experiment, a temperature gradient was applied across the object, with high stresses even at relatively low temperatures. We created two simple holders for the object so that the two sets of experiments could be realized. First, the object was housed in a cylindrical stainless-steel holder padded on the inside with an insulator to prevent heat flow or heat loss through the circumference, thus mimicking the zero-heat-flow boundary condition scenario as shown in Fig. 5(a). This boundary condition results in a uniform temperature even if the heating mechanism is not uniform across the sample. Second, the object was housed in a copper block that was water cooled, so that the boundary was always at a constant temperature, as shown in Fig. 5(b). This boundary condition results in a very strong thermal gradient across the object. The diamond tool sample was laser heated with both laser beam profiles and two optical setups, and then the resultant temperature profile was measured. The temperature was measured in the IR at several discrete wavelengths in the wavelength range between 8 and 14 μm using an uncooled microbolometer (a-Si) (Xenlcs Gobi-1152) IR camera. The number of the camera pixels is 384 to 288 with resolution of 25 μm per pixel. The frame capture rate was fixed at 25 Hz with a 16-bit depth for A-to-D conversion. The camera was calibrated for temperature range from room temperature to 1273 K. During heating, the resulting graybody emission from the sample was collected on an IR camera and converted into a temperature profile using blackbody principles.

3 Results and Discussion

Figure 6 shows thermal images of the insulator holder with the diamond sample inside it and the copper-cooled holder with the diamond sample inside it. Because of the boundary condition of zero heat flow achieved by the setup in Fig. 5(a), the sample takes on a uniform temperature profile even when the source term is not uniform. The predicted profiles for a Gaussian source term are shown in Fig. 1(a), the measured profiles in Fig. 7(a), and similar profiles are found with the use of the flat-top beam. The results show that even with a Gaussian laser beam profile, this setup allows a uniform temperature profile across the PCD sample. Because of the boundary condition of the temperature profile at the edge of the sample being room temperature, achieved by the

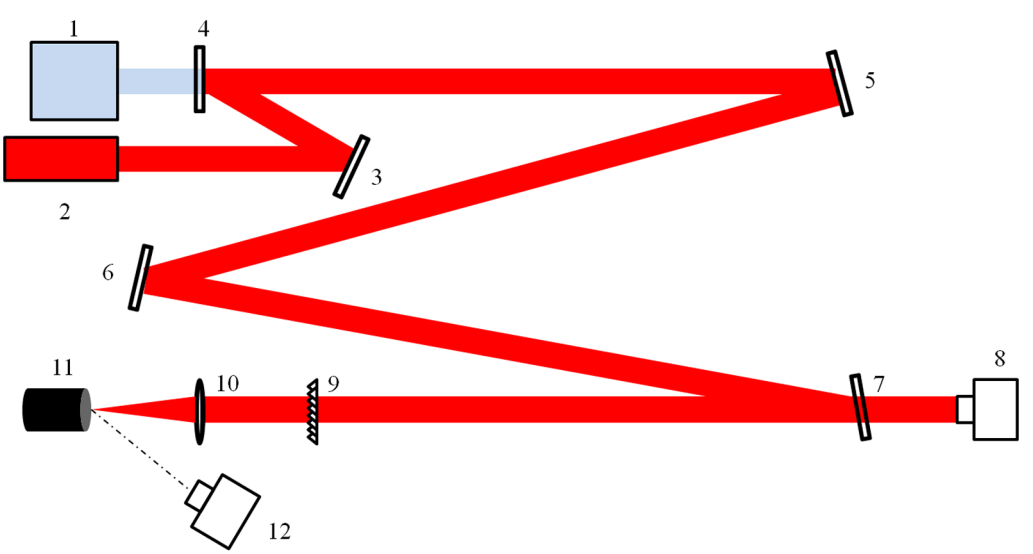

Fig. 3 Schematic drawing of the optical configuration for laser heating of the sample and measuring the resultant temperature. 1, CO_2 laser 10.6 μm; 2, HeNe laser 632.8 nm; 3, $R = 6$-m moly mirror; 5, $R = \infty$ copper mirror; 6, $R = \infty$ copper mirror; 7, ZnSe beam splitter 88% reflection; 8, power meter; 9, diffractive optical element; 10, ZnSe lens $f = 250$ mm; 11, sample; 12, infrared camera.

Downloaded From: http://spiedigitallibrary.org/ on 08/21/2013 Terms of Use: http://spiedl.org/terms

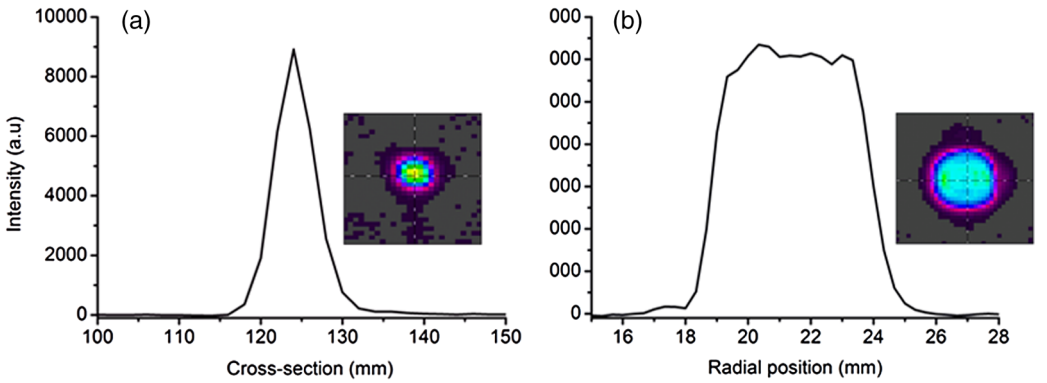

Fig. 4 (a) Gaussian beam profile. (b) Flat-top beam profile.

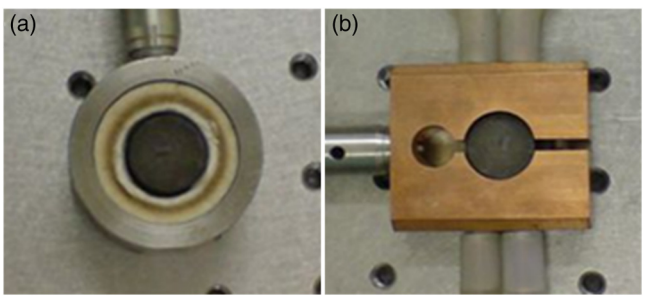

Fig. 5 (a) Insulator holder with the diamond sample inside it. (b) Copper-cooled holder with the diamond sample inside it.

setup in Fig. 5(b), the sample takes on a gradient temperature profile. The predicted profiles for a Gaussian source term are shown in Fig. 1(b) and the measured profiles in Fig. 7(b). The results show that with a Gaussian laser beam profile, this setup allows a gradient temperature across the PCD sample. Previously, it has been shown[34] that laser heating does not result in graphitization of the PCD, but rather cobalt and tungsten oxides form on the diamond surface, as shown in Fig. 8. In Fig. 8, we show two diamond tool samples after laser heating; the laser was focussed at the center of the PCD surface for approximately 8 s at an average laser power of 4 kW using a CO_2 and Nd:YAG laser, respectively. We observe that the thermally induced stresses in the diamond are sufficient to change its physical and chemical properties. X-ray diffraction, Raman spectroscopy, and scanning electron microscopy confirm the diffusion of the cobalt and tungsten from the diamond base, forming oxides at the surface.[34] This accounts for the color changes evident (compared to Fig. 2), while the physical changes are due to thermal stresses and fracture. In such experiments, the thermal gradients could not be controlled, nor was there a suitable system in place for measuring the resulting temperature profile across the sample.

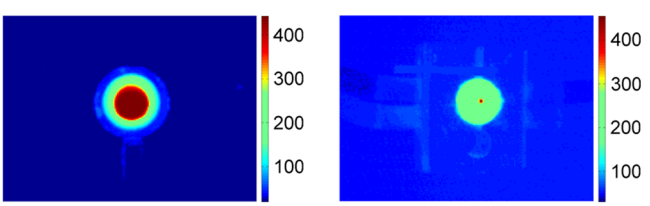

Fig. 6 Thermal images. (a) Insulator holder with the diamond sample inside it. (b) Copper-cooled holder with the diamond sample inside it.

Although there is qualitative agreement between theory and experiment, there is no quantitative agreement. Beside this disagreement, there is a good agreement between the model prediction and the experimental data on the temperature profiles: temperature rises as time increases, temperature increases as the laser beam size decreases, and also temperature increases as the laser beam power increases, as shown in Figs. 1 and 7.

Figures 9 and 10 show a comparison of the Raman spectra and scanning electron microscopy (SEM) micrographs taken on the surface of the PCD layer for the samples shown in Fig. 8. Raman spectra were taken on the PCD layer surface before and after laser heating for 45 min. The sample was heated for 45 min at a laser beam power of 26 W and laser beam radius of 0.7 mm. The temperature was determined to be 681 K by collecting the emitted emission of the diamond tool using the infrared camera. The infrared camera used the emission to determine the temperature using the blackbody principle mentioned above. It is evident that there is no graphitization on the surface of the PCD layer due to the temperature, since there is no peak for graphite on the Raman spectra. However, there are Raman shifts for the peaks of the oxides of W and Co, as seen in Fig. 9. This was also observed on the SEM micrograph of Fig. 10. The SEM micrographs show that the Co and W migrated on the PCD layer, and microstructure was formed due to laser heating or temperature. There is a small Raman shift of the diamond peak (1338 cm^{-1} before and 1335 cm^{-1} after laser heating for 45 min), compared with pure diamond (1332 cm^{-1}).[35] Cappelli et al.[36] observed a similar Raman shift of the diamond peak after growing the diamond tool using chemical vapor deposition (CVD). It was suggested that the shift could be due to some compressive deformation coming from the thermal expansion mismatch between diamond and the hard metal WC substrate ($\alpha_{diamond} \sim 0.8 - 1 \times 10^{-6}$ K^{-1}, compared with $\alpha_{WC.Co} \sim 4.5 - 5.4 \times 10^{-6}$ K^{-1}). In our case, the compressive deformation should be coming from the doping or alloying effects of the Co and W diffusion into diamond. All the Raman shifts were identified based on previous work.[37]

Figure 11 gives the morphology evolution from laser-heated position to the heat-unaffected zone (the base material) of the diamond tool. The inserted SEM morphology displays a close-up view of the interface between the fusion and heat-affected zone. The grain structure of any

Downloaded From: http://spiedigitallibrary.org/ on 08/21/2013 Terms of Use: http://spiedl.org/terms

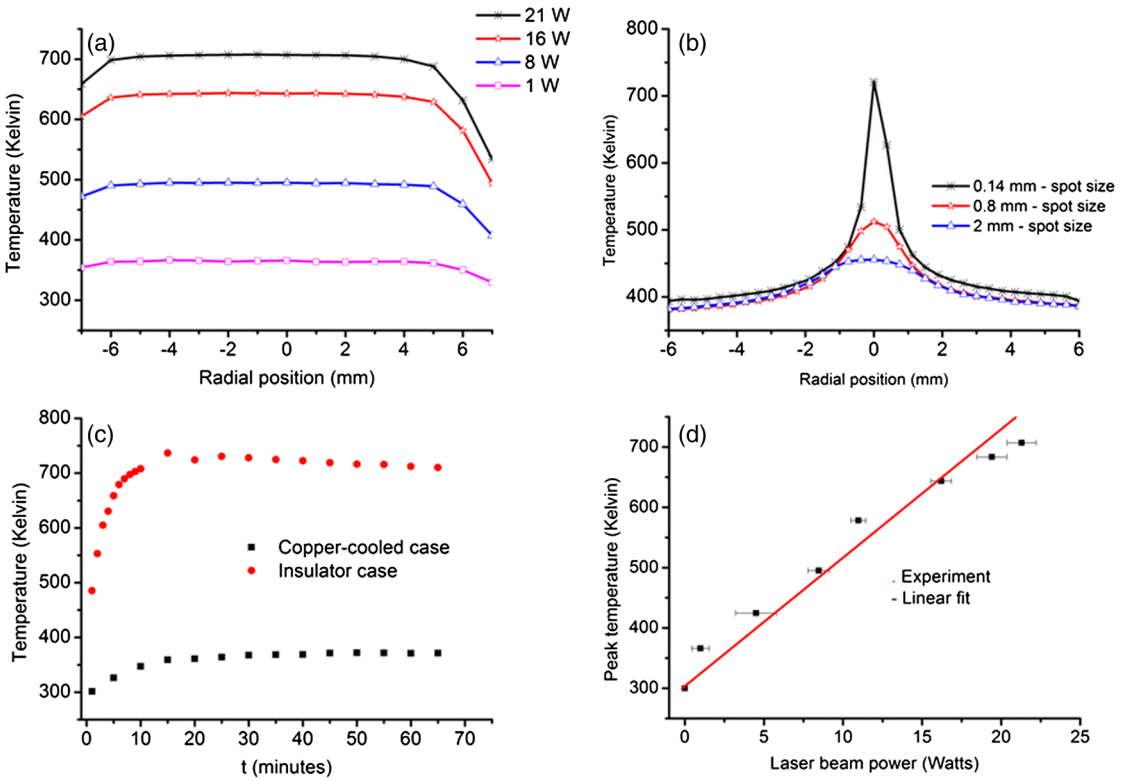

Fig. 7 Temperature profile across the sample surface per laser beam power or time for the sample that was laser heated with the Gaussian laser beam profile and flat-top laser beam profile. (a) Insulator holder results. (b) Copper-cooled holder results. (c) For both cases, temperature rises as time increases and stabilizes after a few minutes. (d) For both cases, temperature rises as laser beam power increases.

solid material changes during laser heating, as shown in Fig. 11. It is subjected to the peak temperatures that are higher than the melting point of the materials, followed by rapid cooling. The efficacy of the diamond tool decreases rapidly at temperatures exceeding 700°C to 750°C during a typical drilling process due to friction.[32] In this SEM morphology (Fig. 11), the peak temperature was measured to be 853 K and was then rapidly cooled. These temperature fluctuations change the microstructure of the material non-uniformly to create the heat-affected zone next to the fusion zone, as shown in inset SEM morphology of Fig. 11. Within the heat-affected zone, the most severe microstructural changes occur close to the fusion zone, where the peak temperatures are the highest.[38] The partially melted zone (fusion zone) is rather narrow, only several tens of micrometers, and of a scale similar to the heat-affected zone. Crack growth was observed in the fusion zone, as shown in the inset SEM morphology image.

Comparing the average and peak temperature values, the thermally induced stresses in the diamond are minimized, yet the temperature experienced by the diamond can be arbitrarily large, thus allowing a controlled study of the physical and chemical changes in diamond due to heating alone. Previously, such studies were conducted in hot filaments,[39] diamond anvil cells (DACs),[40] and microwave plasma.[41] In this work, the same effect was created with the added advantage of localized heating down to the diffraction limit of the

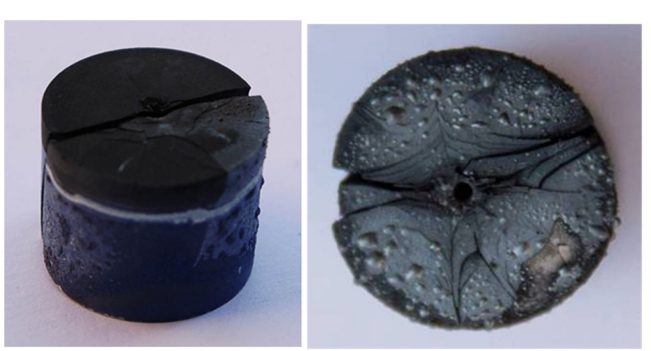

Fig. 8 Diamond tools damaged by the laser heating, with both physical and chemical changes evident.

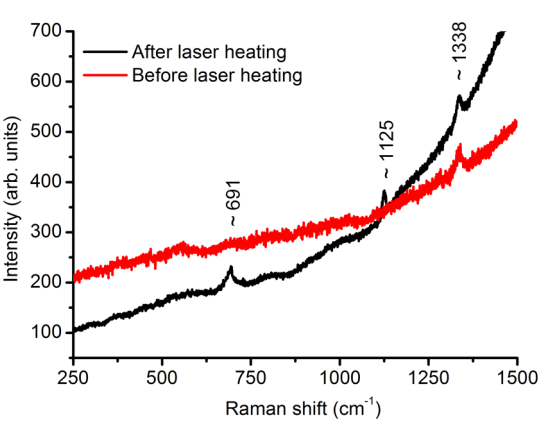

Fig. 9 Initially, the PCD layer shows a Raman shift around 1338.2 cm^{-1}, which is a diamond peak, and after laser heating for 45 min, the PCD layer shows some Raman shift of Co or W oxides and the diamond peak has shifted to 1335 cm^{-1} on the diamond layer, caused by the laser heating. The temperature was determined to be 681 K.

Downloaded From: http://spiedigitallibrary.org/ on 08/21/2013 Terms of Use: http://spiedl.org/terms

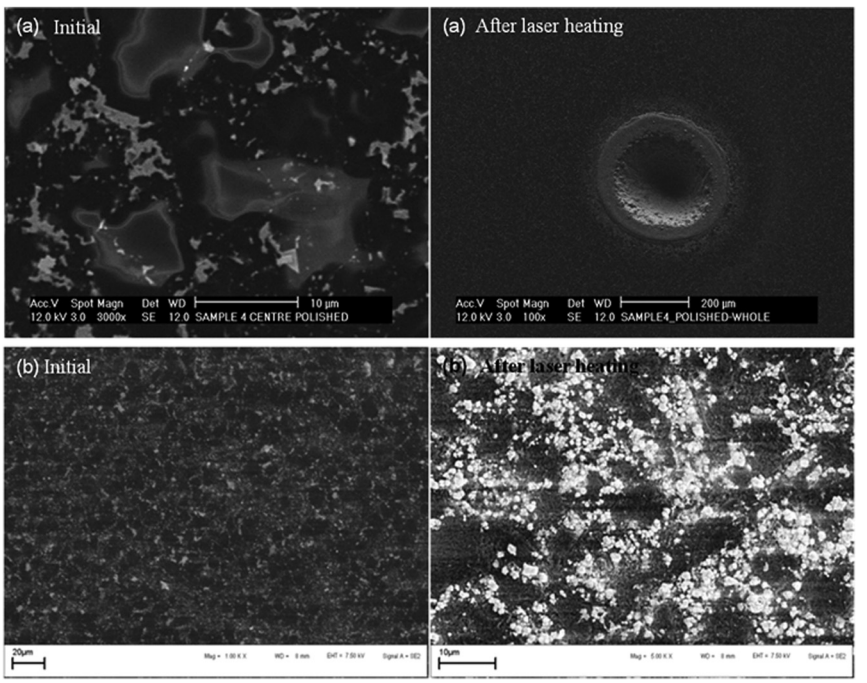

Fig. 10 (a) SEM morphology for the copper-cooled case, showing only the damage where the laser was heating the diamond layer (peak temperature 853 K, laser power 242 W, beam radius 0.14 mm, heating duration 30 s). (b) SEM morphology for the insulator case, showing uniform damage on the diamond layer after laser heating (peak temperature 681 K, laser power 26 W, beam radius 0.7 mm, heating duration 45 min).

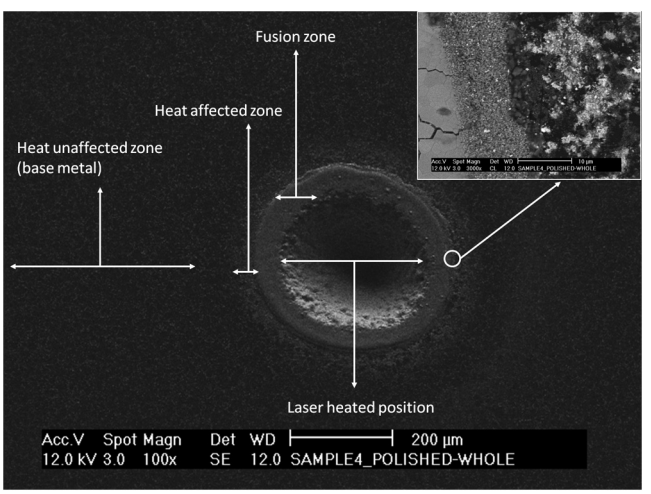

Fig. 11 SEM morphology for the copper-cooled case, showing the damage where the laser was heating the diamond layer, fusion zone, heat-affected zone, and heat-unaffected zone (peak temperature 853 K, laser power 242 W, beam radius 0.14 mm, heating duration 30 s). Inset: Morphology was taken at the edge of the fusion zone and shows the fusion-zone line and the heat-affected-zone structure.

laser beam spot size, thus opening the way to controlled spatial studies on diamond-heated samples.

4 Conclusion

We have demonstrated a laser beam shaping system for heating and then measuring the temperature profile of a particular diamond tool sample. However, this system can be used for any material. We successfully raised the temperature profile of the sample in a controllable manner over a wide range of laser powers and showed that a uniform and gradient temperature profile across the sample could be engineered. The experimentally measured profiles are in qualitative agreement with those predicted theoretically, while we can measure the temperature of a sample to within 1 K from just above room temperature to >1000 K without contact with the sample. The creation of such temperature profiles allows a study of temperature influences without and with thermal stress, adding a valuable tool for those wishing to execute controlled material heating studies.

Acknowledgments

We thank Bafana Moya for his technical assistance.

References

1. R. R. Cavanagh, D. S. King, and J. C. Stephenson, "Dynamics of non-thermal reactions: femtosecond surface chemistry," *J. Phys. Chem.* **97**(4), 786–798 (1993).
2. L. C. Ming and W. A. Bassett, "Laser heating in the diamond anvil press up to 2000°C sustained and 3000°C pulsed at pressures up to 260 kilobars," *Rev. Sci. Instr.* **45**(9), 1115–1118 (1974).
3. O. U. Khan and B. S. Yilbas, "Laser heating of sheet metal and thermal stress development," *J. Mater. Proc. Tech.* **155–156**, 2045–2050 (2004).
4. J. B. Cui, K. Amtmann, and J. Ristein, "Non-contact temperature measurements of diamond by Raman scattering spectroscopy," *J. Appl. Phys.* **83**(12), 7929–7933 (1998).
5. L. S. Dubrovinsky and S. K. Saxen, "Emissivity measurements on some metals and oxides using multi-wavelength spectral radiometry," *High Temp. High Pres.* **31**(4), 393–399 (1999).
6. S. Keyvan, R. Rossow, and C. Romero, "Blackbody-based calibration for temperature calculations in the visible and near-IR spectral ranges using a spectrometer," *Fuels* **85**(5–6), 796–802 (2006).
7. G. Barrow, "Review of experimental and theoretical techniques for assessing cutting temperatures," *Ann. CIRP* **22**(2), 203–211 (1973).
8. P. R. N. Childs, J. R. Greenwood, and C. A. Long, "Review of temperature measurement," *Rev. Sci. Instr.* **71**(8), 2959–2978 (2000).
9. M. A. Davies et al., "On the measurement of temperature in material removal processes," *Ann. CIRP Manu. Tech.* **56**(2), 581–604 (2007).
10. M. H. Attia, A. Cameron, and L. Kops, "Distortion in thermal field around inserted thermocouple in experimental interfacial studies, Part 4: end effect," *J. Man. Sci. Eng.* **124**(1), 135–145 (2002).
11. M. H. Attia and L. Kops, "Distortion in the thermal field around inserted thermocouples in experimental interfacial studies. III: experimental and numerical verification," *J. Eng. Ind.* **115**(4), 444–449 (1993).

Downloaded From: http://spiedigitallibrary.org/ on 08/21/2013 Terms of Use: http://spiedl.org/terms

12. G. Byrne, "Thermoelectric signal characteristics and average interfacial temperature in the machining of metals under geometrically defined conditions," *Int. J. Mach. Tools Manu.* **27**(2), 215–224 (1987).
13. D. A. Stephenson, "Assessment of steady-state metal cutting temperature models based on simultaneous infrared and thermocouple data," *ASME J. Eng. Ind.* **113**(2), 121–128 (1991).
14. C. Lempereur, R. Andral, and J. Prudhomme, "Surface temperature measurement on engine components by means of irreversible thermal coatings," *Meas. Sci. Technol.* **19**(10), 104903 (2008).
15. S. A. Allison and G. T. Gillies, "Remote thermometry with thermographic phosphors: instrumentation and applications," *Rev. Sci. Instr.* **68**(7), 2615–2650 (1997).
16. J. Brübach et al., "On surface temperature measurements with thermographic phosphors: a review," *Prog. Energy Combust. Sci.* **39**(1), 37–60 (2013).
17. S. Elhadj et al., "High temperature thermographic measurements of laser heated silica," *Proc. SPIE* **7504**, 750419 (2009).
18. S. T. Yang et al., "Thermal transport in CO_2 laser irradiated fused silica: in situ measurements and analysis," *J. Appl. Phys.* **106**(10), 103106 (2009).
19. Z. M. Zhang, "Surface temperature measurement using optical techniques," in *Annual Review of Heat Transfer Online*, V. Prasad, Y. Jaluria, and G. Chen, Eds., Vol. 8, pp. 351–411, Begell, Redding, CT (1997).
20. J. Hartmann, "High-temperature measurement techniques for the application in photometry, radiometry and thermometry," *Phys. Rep.* **469**(5–6), 205–269 (2009).
21. F. M. Dickey and S. C. Holswade, *Laser Beam Shaping: Theory and Techniques*, Marcel Dekker, New York (2000).
22. W. Lee, "Method for converting a Gaussian laser beam into a uniform beam," *Appl. Opt.* **22**(6), 3644–3647 (1983).
23. K. Kanzler, "Diffractive laser beam shaping for material processing using a CO_2 laser," *Proc. SPIE* **5525**, 64–75 (2004).
24. A. Forbes et al., "Wavelength tunable laser beam shaping," *Opt. Lett.* **37**(1), 49–51 (2012).
25. H. S. Carslaw and J. C. Jaeger, *Conduction of Heat in Solids*, Clarendon Press, Oxford, UK (1959).
26. B. N. Masina, "Optical determination of the temperature of a laser heated industrial diamond," MSc Dissertation, pp. 39–56, University of Zululand (2008).
27. G. B. Arfken and H. J. Weber, *Mathematical Methods for Physicists*, 4th ed., p. 385, Academic Press, New York (1995).
28. H. D. Young, *University Physics*, 8th ed., p. 5290, Addison-Wesley, New York (2008).
29. E. H. Bernhardi et al., "Estimation of thermal fracture limits in quasi-continuous-wave end-pumped lasers through a time-dependent analytical model," *Opt. Express* **16**(15), 11115–11123 (2008).
30. G. Barton, *Elements of Green's Functions and Propagation*, pp. 41–75, Oxford University Press, Oxford, UK (1995).
31. S. -M. Hong et al., "Dissolution behaviour of fine particles of diamond under high pressure sintering conditions," *J. Mater. Sci. Lett.* **10**(3), 164–166 (1991).
32. V. Prakash and F. C. Appl, "Temperature distribution in synthetic diamond cutters during orthogonal rock cutting," *SPE Drill. Eng.* **4**(2), 137–143 (1989).
33. R. G. Wentorf, R. C. DeVries, and F. P. Bundy, "Sintered superhard materials," *Science* **208**(4446), 873–880 (1980).
34. B. N. Masina et al., "Thermally induced defects in a polycrystalline diamond layer on a tungsten carbide substrate," *Phys. B* **404**(22), 4485–4489 (2009).
35. S. A. Catledge et al., "Micro-Raman stress investigations and X-ray diffraction analysis of polycrystalline diamond (PCD) tools," *Diamond Related Mater.* **5**(10), 1159–1165 (1996).
36. E. Cappelli et al., "Diamond nucleation and growth on different cutting tool materials: influence of substrate pre-treatments," *Diamond Related Mater.* **5**, 292–298 (1996).
37. J. Diaz-Reyes et al., "Obtaining of films of tungsten trioxide (WO_3) by resistive heating of a tungsten filament," *Superficies Vacio* **21**(2), 12–17 (2008).
38. X. Cao et al., "A review of laser welding techniques for magnesium alloys," *J. Mater. Pro. Tech.* **171**, 181–204 (2006).
39. Y. H. Lee et al., "Vapor deposition of diamond thin films on various substrates," *Appl. Phys. Lett.* **57**(18), 1916–1919 (1990).
40. D. L. Heinz and J. S. Sweeney, "Al laser heating system that stabilizes and controls the temperature: diamond anvil cell applications," *Rev. Sci. Instr.* **62**(2), 1568–1575 (1991).
41. S. A. Stuart, S. Prawer, and P. S. Weiser, "Growth-sector dependence of fine structure in the first-order Raman diamond line from large isolated chemical-vapor-deposited diamond crystals," *Appl. Phys. Lett.* **62**(11), 1227–1230 (1993).

Bathusile N. Masina is a researcher within the Advanced Photonic Materials laboratory at the CSIR National Laser Centre in Pretoria, South Africa. She received an MSc (2008) in physics in the University of Zululand, Empangeni, South Africa. She is presently pursuing her PhD in the University of KwaZulu-Natal, Durban, South Africa.

Biographies and photographs of the other authors are not available.

Downloaded From: http://spiedigitallibrary.org/ on 08/21/2013 Terms of Use: http://spiedl.org/terms